Nuclear Magnetic Resonance – An Overview

Ali Ahmed, Zain Kamal, and Neil Mandar
Department of Physics & Astronomy, Rutgers University
(Dated: May 6, 2025)

This report summarizes our investigation of pulsed nuclear magnetic resonance (NMR) using the TeachSpin spectrometer. Building on the principles of Larmor precession and the quantum-mechanical behavior of spin-½ nuclei, we examined the response of magnetic moments when subjected to time-dependent radio frequency (RF) pulses. We began with a theoretical framework covering key concepts such as the net magnetization arising from the Boltzmann population difference and the associated longitudinal (T_1) and transverse (T_2) relaxation processes. In our experiments, specially-tuned $\frac{\pi}{2}$ and π pulses were applied to tip and invert the magnetization, thereby generating free induction decay (FID) signals and spin echoes. A simulation model incorporating the exponential decay of echo amplitudes provided a basis for comparing the expected with the observed signal features. Data analysis of envelope decay yielded T_1 and T_2 times for mineral oil, water, and glycerol. Our study demonstrates the successful application of pulsed NMR techniques in measuring relaxation times, validating both the theoretical description and the simulation model.

I. INTRODUCTION AND THEORETICAL DESCRIPTION

The study of nuclear magnetic resonance (NMR) utilizes weak magnetic fields to affect the nuclei of atoms in a strong magnetic field. Under certain conditions, atoms will exhibit "resonance," causing the observation of a transient magnetic field as nuclei relax back to their equillibrium state.

A. Larmor Precession

We will start with the phenomena of Larmor precession, occuring when atoms are placed in a strong magnetic field. Larmor precession most readily occurs when the nucleus has a net magnetic moment i.e. there is an odd number of nucleons (protons and neutrons), producing a spin ½ system (e.g. ^1H, ^{13}C, ^{19}F, etc.). In this case, the magnetic dipole moment μ of the nucleus is described as

$$\vec{\mu} = \gamma \vec{S} \tag{1}$$

where $\vec{S}$ denotes the spin vector and γ is a constant known as the gyromagnetic ratio (which differs depending on the type of nucleus). Under a magnetic field, the energy of this system reads

$$E = -\vec{\mu} \cdot \vec{B_0} \tag{2}$$

where we denote B_0 the external magnetic field. This yields the Hamiltonian

$$H = -\gamma \vec{B_0} \cdot S \tag{3}$$

where S is the Pauli spin operator $S = (\sigma_x, \sigma_y, \sigma_z)$. Let us orient our magnetic field against the z-axis, such that

$$\vec{B_0} = B_0 \hat{z} \tag{4}$$

and the Hamiltonian now reads

$$H = -\frac{\hbar}{2}\gamma B_0 \begin{pmatrix} 1 & 0 \\ 0 & -1 \end{pmatrix} \tag{5}$$

The Hamiltonian has eigenstates

$$|\pm\rangle : E_\pm = \mp\frac{\hbar}{2}\gamma B_0 \tag{6}$$

These eigenstates correspond to nuclei aligned either parallel or antiparallel to the magnetic field B_0. We will use these vectors $|\pm\rangle$ as our basis. We can evolve these stationary states with the time-dependent Schrödinger equation and then calculate the expectation of each of our Pauli matrices to obtain

$$\begin{aligned} \langle S_x \rangle &= \frac{\hbar}{2}\sin(\theta)\cos(\gamma B_0 t) \\ \langle S_y \rangle &= \frac{\hbar}{2}\sin(\theta)\sin(\gamma B_0 t) \\ \langle S_z \rangle &= \frac{\hbar}{2}\cos(\theta) \end{aligned}$$

These equations are the classical precession equations; our spin vector will precess about the magnetic field at a constant frequency

$$\omega_0 = \gamma B_0 \tag{7}$$

This frequency is known as the **Larmor frequency**, and θ indicates the angle between $\vec{\mu}$ and $\vec{B_0}$. [1]

θ characterizes the system, up to a phase,

$$|\psi\rangle = \cos(\theta/2)\,|+\rangle + e^{i\phi}\sin(\theta/2)\,|-\rangle$$

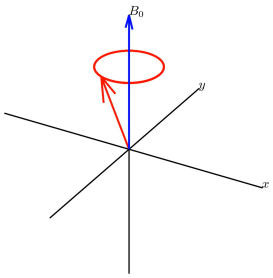

FIG. 1: Larmor precession about $\vec{B_0}$

These equations above can also be derived from a classical viewpoint; we can calculate the torque $\vec{\tau} = \vec{\mu} \times \vec{B_0}$ on the nucleus by the magnetic moment and use Newton's second law to derive a similar precession.

B. Net Magnetization and Relaxation

The lower energy E_+ is the favored energy state; slightly more spins will align parallel to $\vec{B_0}$ as opposed to antiparallel. Using statistical mechanics, we can derive the expected number of $|+\rangle$ vs $|-\rangle$. Since this is a canonical two-state system, the ratio $\frac{N_+}{N_-}$ is equal to the ratio of the Boltzmann factors, yielding

$$\frac{N_+}{N_-} = \exp\left(\frac{\gamma \hbar B_0}{kT}\right) \tag{8}$$

This small difference produces a net longitudinal magnetization (in this context, "longitudinal" refers "along the B_0 field"), which is the sum of the individual quantized spins of the sytem. [2]

$$M_z = \sum_i \gamma \hbar m_i = \frac{\hbar}{2}\gamma(N_+ - N_-) \tag{9}$$

In equillibrium with our original magnetic field B_0, we expect a slight magnetization in the $+\hat{z}$ direction. However, if we were to apply another magnetic field briefly to this system, we would see a change in the net magnetization $\vec{M}(t)$. Eventually, the system will return back to its equillibrium state. In order to reach equillibrium, the system must give back energy to the surrounding lattice.

We are interested in understanding how long it takes for our system to reach equillibrium. In general, after a disturbance, the magnetization follows the Bloch equation, reproduced in Equation 10.

$$\frac{d\vec{M}(t)}{dt} = \frac{\vec{M}(t) - \vec{M}_0}{T_1} \tag{10}$$

where $\vec{M}_0$ denotes the equillibrium magnetization. We refer to T_1 as the **spin-lattice relaxation time**. [3]

One can solve Equation 10 to yield

$$M_j(t) = M_0 - (M_0 - M_i)e^{-t/T_1} \tag{11}$$

where M_0 is the magnetization at equillibrium and M_i is the initial magnetiztion.[3] This formulation will be useful later when performing experiments.

C. Producing Transverse Magnetizations

1. *Apply a Circularly Polarized Field*

So far, we have discussed the uniform $\vec{B_0}$ field. However, to produce a transverse magnetization (i.e. a magnetization in the x-y plane) we need to get creative. We will use a circularly polarized field,

$$\vec{B_1}(t) = B_1\left[\cos(\omega_0 t)\hat{x} + \sin(\omega_0 t)\hat{y}\right] \tag{12}$$

Note that $\vec{B_1}(t)$ oscillates at the Larmor frequency. Thus, the new Hamiltonian has an extra time-dependant term, still in the form of Equation 3. Solving this Hamiltonian is beyond the scope of this lab report; however, we can still apply the classical torque result to obtain [3]

$$\vec{\tau} = \vec{\mu} \times \left[\vec{B_0} + \vec{B_1}(t)\right] \tag{13}$$

by transforming into a rotating reference frame (rotating at the Larmor frequency), we find that the effective field becomes

$$\vec{B^*} = (B_0 - \mu/\gamma)\hat{z}^* + B_1\hat{x}^* \tag{14}$$

In this rotating frame, applying a circularly polarized magnetic field has the effect of "tipping" the magnetization into a transverse plane. Transforming back into the lab frame, we will observe the magnetization in the x-y plane still precessing about the z-axis.

2. $\frac{\pi}{2}$ *and* π *pulses*

By applying $\vec{B_1}(t)$, we will create two types of pulses. We will first define a $\frac{\pi}{2}$ **pulse**, a pulse of $B_1(t)$ that will be applied for exactly long enough such that the magnetization is entirely in the $x-y$ plane. We will also define a π **pulse**, a pulse that flips the magnetization from $+\hat{z}$ to $-\hat{z}$.

During a $\frac{\pi}{2}$ or π pulse, we can plot the expectation $\langle\vec{S}\rangle = (\langle S_x\rangle, \langle S_y\rangle, \langle S_z\rangle)$ over time, as shown in Figure 2.

As a practical matter, the Larmor frequency generally lies in the radio frequency range for most atoms. As a result, the $\vec{B_1}(t)$ pulses are referred to as **RF pulses**.

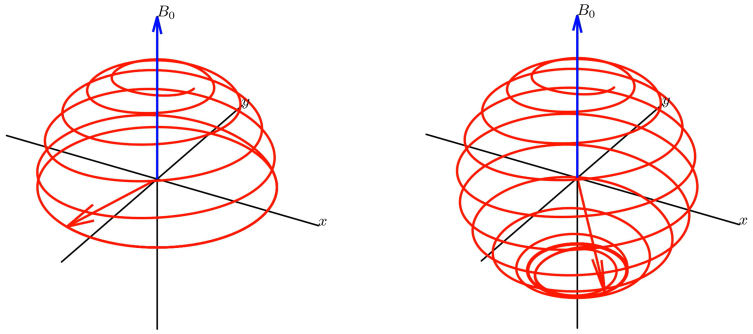

(a) $\frac{\pi}{2}$ pulse produces transverse magentization

(b) π pulse flips magentization from $+\hat{z}$ to $-\hat{z}$

FIG. 2: $\langle \vec{S} \rangle$ over time during a $\frac{\pi}{2}$ and π pulse

D. Spin-Spin Relaxation

Along with the decay of the transverse magnetization, we observe a different kind of decay; the decay of the relative phasing of all of the magnetic moments. After a $\frac{\pi}{2}$ pulse, the magnetic moments are in phase with each other—however, due to mutual interactions, these moments slowly turn out of phase. This dephasing is known as **spin-spin relaxation**, and obeys a similar relationship to Equation 10. In particular, the external magnetic field denoted by $\vec{M}_0$ in Equation 10 is $\vec{0}$. Adapting this, we obtain Equation 15.

$$\frac{d\vec{M}_{x,y}}{dt} = \frac{\vec{M}_{x,y}}{T_2} \tag{15}$$

Note that both Equation 10 and 15 are in the same form, following a familiar exponential curve.

E. Free Induction Decay and T_2^*

Suppose we apply a $\frac{\pi}{2}$ pulse to a system of nuclei; the net magnetization will be in the x-y plane. Further suppose we place this sample within a coil aligned in either the x or y direction. Since this magnetization is precessing at the Larmor frequency about $\vec{B}_0$, the moment induces a change in flux in the coil, producing a periodic voltage we can measure.

This oscillation will decay according to Equations 10 and 15 as the magnetization becomes increasingly decoherent. The envelope of this decay is known as **free induction decay (FID)**.

The characteristic decay time constant of an FID signal depends not only on T_1 and T_2, but also local inhomogeneities in $\vec{B}_0$. We label the time constant obtained from all three factors T_2^*, which, with some simple algebra, we obtain as [2]

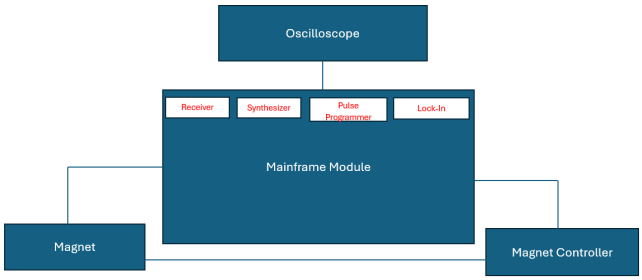

FIG. 3: TeachSpin NMR Apparatus

$$\frac{1}{T_2^*} = \frac{1}{T_1} + \frac{1}{T_2} + \gamma \Delta B_0 \tag{16}$$

In order to directly measure T_1 and T_2, we must therefore get creative on our measurement techniques. By using specific pulse sequences (see Section IIA,B), the effects of the $\gamma \vec{\Delta} B_0$ can be mitigated and T_1 and T_2 can be isolated and calculated using Equations 10 and 15, respectively.

II. APPARATUS AND EXPERIMENTAL PROCEDURE

The apparatus for NMR experiments (Figure 3) consists of a TeachSpin PS2-B Pulsed/CW NMR set and a Tektronix oscilloscope. The TeachSpin set comes with a 0.49 T permanent magnet, PS2 magnet temperature controller, and mainframe module with pulse programmer, synthesizer, receiver and lock-in amplifier. The synthesizer generates the signal that will be used to excite proton spins. The receiver reads the signal (specifically the envelope of the signal) from a pickup coil aligned with $+\hat{x}$ of the permanent magnet; this coil outputs a voltage

when proton spins produce a net change of flux. The oscilloscope then displays the output from the receiver. The pulse programmer allows for the length, period and delay time to be set for a pulse sequence. This will be critical in creating the sequences of $\frac{\pi}{2}$ and π pulses needed to effectively measure NMR decay.

It is critical that the frequency of the RF signal be tuned to match the Larmor frequency of protons in the static magnetic field. For hydrogen, the Larmor frequency is 21 MHz.

A. Measuring T_1

There are two traditional pulse sequences that allow for a T1 measurement: $\frac{\pi}{2}$ and $\pi - \frac{\pi}{2}$. By applying a single $\frac{\pi}{2}$ pulse, the net magnetization vector is tipped into the x-y plane, producing an FID signal. This signal quickly decays primarily due to the dephasing of individual spins, but also realignment of spins with $+\hat{z}$. Even after this signal disappears, the net magnetization vector is still decaying towards $+\hat{z}$. At any moment in time, another $\frac{\pi}{2}$ pulse can be applied. When this happens, any spins aligned with the $+\hat{z}$ are thrown back in the x-y plane and can be measured, while those in the x-y plane are rotated out of the measurement region. This means that by applying two $\frac{\pi}{2}$ pulses, one can effectively check the decay of net magnetization and characterize it with a time constant.

Alternatively, one can apply a π pulse, which inverts the net magnetization to $-\hat{z}$. This produces a negligible FID signal, since the spins dephase before entering the measurement region (x-y plane). In spite of this, the net magnetization vector is still decaying towards $+\hat{z}$. At any moment in time, a $\frac{\pi}{2}$ pulse can be applied to, much like before, check the decay of the net magnetization. When the FID signal following a $\frac{\pi}{2}$ pulse is zero, half of the spins have decayed back to $+\hat{z}$. This is known as the **zero crossing time** and can be used to calculate the time constant of the decay. This method is preferred, since a null signal can easily be identified.

B. Measuring T_2

T2 measurements require a $\frac{\pi}{2} - \pi$ pulse sequence. The $\frac{\pi}{2}$ pulse tips the magnetization into the x-y plane, where the spins dephase due to inhomogeneities in the static magnetic field and spin-spin interactions. The goal in a T2 measurement is to isolate the spin-spin dephasing. To do this, one must note that magnitude of spin dephasing is related to the strength of the static field it experiences. When a spin is kicked into the x-y plane, torque from the static magnetic field forces it to rotate in that plane. Spins in a stronger magnetic field rotate more quickly than ones in a weaker magnetic field, leading to aggressive dephasing. To mitigate this, a π pulse is applied. The π pulse essentially flips the direction of spin rotation, meaning all spins rotate back at roughly the same speed.

This leads to the 'rephasing' of spins shortly after the pulse since spins that rotated more quickly following the $\frac{\pi}{2}$ pulse have a longer distance to travel on the way back after the π pulse. This rephasing is known as a **spin echo**. If the inhomogeneous field were the only cause of dephasing, the magnitude of the rephased signal would equal the initial in phase signal. However, since spin-spin interactions are also dephasing spins, the rephased signal is slightly weaker. By applying multiple π pulses after an initial $\frac{\pi}{2}$ pulse, one can track the decay in magnitude of the rephasing signal due to spin spin interactions and characterize it with a time constant, this time constant is T2.

It's important that the π pulses are close together, since particle diffusion in a sample can cause a proton to move into a different magnetic field region. This would make the 'rephasing' speed of the spin different from its initial 'dephasing' speed, causing it to not rephase with other spins for reasons not related to the spin-spin interactions we seek to measure.

III. RESULTS & DISCUSSION

A. Measuring T_1

To determine the spin-lattice relaxation time T_1 for all three samples, we employed the inversion-recovery (π-τ-$\pi/2$) sequence described in Section II A. In each measurement:

1. A 180° (π) pulse inverts the equilibrium magnetization:

$$M_0\hat{z} \longrightarrow -M_0\hat{z}\,. \tag{17}$$

2. After a variable delay τ, a 90° ($\pi/2$) pulse rotates the recovered longitudinal magnetization into the transverse plane:

$$M_z(\tau) \longrightarrow M_{xy}(0)\,, \tag{18}$$

   whose amplitude is then detected as the initial free induction decay (FID).

3. We record the delay $\tau = t_{\text{cross}}$ at which the FID amplitude first crosses zero ($M_z = 0$), corresponding to equal spin populations:

$$\frac{N_+}{N_-} = 1\,. \tag{19}$$

At the zero-crossing point, substituting $M_i = -M_0$ and $M_z(t_{\text{cross}}) = 0$ into the recovery law

$$M_z(t) \;=\; M_0\big(1 - 2\,e^{-\,t/T_1}\big) \tag{20}$$

yields

$$T_1 = \frac{t_{\text{cross}}}{\ln 2}. \tag{21}$$

No oscilloscope trace is shown at the null point, since the baseline is indistinguishable from zero signal. The measured crossing delays and corresponding T_1 values are:

TABLE I: Zero-crossing delays and extracted T_1 values for each compound.

Compound	t_{cross} (ms)	T_1 (ms)
Mineral oil	34.0(5)	49.1(7)
Glycerin	28.0(5)	40.4(7)
Deionized water	1300(10)	1880(15)

These results span three orders of magnitude: mineral oil exhibits an intermediate $T_1 \approx 50$ ms, glycerin a slightly shorter $T_1 \approx 40$ ms, and deionized water a very long $T_1 \approx 1.9$ s. This trend reflects each liquid's molecular environment and mobility, as discussed in the Conclusion.

B. Measuring T_2

Now, we can attempt to measure T_2. We will use the $\frac{\pi}{2} - \pi$ sequence outlined in Section II B. As mentioned previously, we apply one $\frac{\pi}{2}$ pulse, and then apply many π pulses to isolate the spin-spin interaction (as opposed to effects caused by the inhomogeneity of the field). This produces spin echoes with decaying magnitude; this is known as the **Carr-Purcell sequence**.

1. *Simulating the Carr-Purcell Sequence*

As the individual spins precess around $\vec{B}_0$, they will continue to rephase until reaching a maximum spin echo. This produces a periodic flux in the pickup coil with peaks, modeled by Equation 22

$$A(n) = A_0 \exp\left(\frac{-t_n}{T_2}\right) \cdot \left[\frac{1}{2}\left(1 + \cos\left(\frac{2\pi n}{\text{beat period}}\right)\right)\right] \tag{22}$$

for $t_n = n \times$ echo_spacing. We define a continuous version by replacing the discrete index n with t/echo_spacing.

From a heuristic standpoint, this makes sense; we have a decaying envelope characterized by $\exp(t_n/T_2)$ and beating following the periodic oscillation of the magnetization.

Plotting these results, we obtain Figure 4.

Why does this look different from the actual data we observe later on? In practice, the NMR receiver first band-limits the raw RF voltage at the Larmor frequency, then mixes it with a local oscillator to bring it down to an intermediate (or baseband) frequency. This down-converted signal is passed through a rectifier (often a precision diode or active circuit) which charges a capacitor on each RF peak, and a resistor then discharges the capacitor between peaks, forming a simple RC low-pass filter that smooths out the tens-of-MHz oscillations and "follows" only the slowly varying amplitude envelope. The result of this envelope detector is a voltage proportional to the magnitude of the transverse magnetization (i.e., the echo amplitude), with all of the high-frequency carrier components removed. Because the oscilloscope displays this low-frequency envelope (not the raw RF oscillations) the observed signal is a smooth, exponentially decaying curve whose time constant directly reflects spin-spin dephasing (T_2) and any beat modulation, rather than the "spiky" substructure of each individual echo.

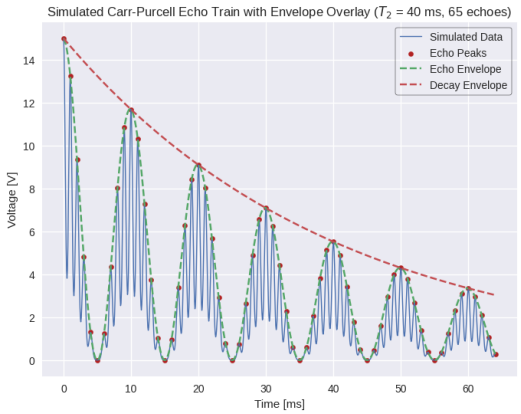

FIG. 4: Simulation of the beating behavior in a Carr-Purcell sequence with 60 π pulses. Each echo is modeled as a Gaussian pulse. The echo amplitude decays exponentially (simulating T_2 decay) and is modulated by a cosine factor (to incorporate beating effects). Additionally, we overlay a smooth envelope curve that passes through the echo peak amplitudes.

2. *Obtaining experimental values of T_2*

We will now create the Carr-Purcell sequence with each sample. Starting from thermal equilibrium, we apply a $\pi/2$ pulse followed by N equally spaced π pulses (the echo spacing is 2τ). For mineral oil, glycerin, and deionized water we performed echo trains with $N \approx \{10, 20, 50\}$ (oil), $N \approx \{20, 30, 50\}$ (glycerin), and $N \approx \{100\}$ (water), using various τ values chosen to maintain sufficient echo amplitude while minimizing diffusion effects.

Because the transverse magnetization in the rotating frame decays as

$$M_{xy}(t) = M_0 \exp\left(-t/T_2\right), \tag{23}$$

we fit an exponential envelope to each echo train to extract T_2. The individual fits are summarized in Table II. To visualize the overall reproducibility, we then compute the mean and standard deviation of all T_2 values for each compound (Table III).

TABLE II: Relaxation parameters for mineral oil, glycerin, and deionized water.

Compound	N	τ (ms)	T_2 (ms)
Mineral oil	10	0.0719	48.8
	20	0.0342	41.1
	21	0.1640	44.7
	50	0.0882	41.3
Glycerin	20	0.0761	27.3
	31	0.0780	27.7
	35	0.0204	28.5
	50	0.0196	27.6
Deionized water	98	1.1600	777.0
	100	0.5940	926.0

TABLE III: Mean and standard deviation of T_2 for each compound.

Compound	Mean (ms)	Std. dev. (ms)
Glycerin	27.8	0.5
Mineral oil	44.0	3.6
Water	851	105

After fitting, we see that glycerin exhibits the shortest transverse relaxation time, with a mean $T_2 = 27.8\,\text{ms}$ and a small relative spread ($< 2\%$), reflecting its highly viscous, hydrogen-bonded environment that rapidly dephases spins. Mineral oil yields an intermediate mean value, $T_2 = 44.0\,\text{ms}$, with moderate variability ($\sim 8\%$), consistent with its nonpolar aliphatic chains and faster molecular tumbling that partially averages dipolar interactions. Deionized water's T_2 is over an order of magnitude larger, 851 ms, albeit with a larger absolute standard deviation due to its long coherence being more sensitive to diffusion and residual field inhomogeneities over extended echo trains.

These results follow the expected trend that slower molecular motion and stronger dipole-dipole couplings (as in glycerin) shorten T_2, while fast tumbling and motional narrowing (as in water) prolong coherence. The Carr-Purcell exponential fits are robust across different N and τ, validating this pulse sequence as an effective method for isolating T_2 in the presence of static field inhomogeneities.

C. Interpreting Results

For context, literature reference values at similar field strength ($\sim$20 MHz) are: water $T_1 \approx$ 3-4 s, glycerin T_1 $\sim$40-50 ms, mineral oil T_1 $\sim$50-60 ms (with T_2 generally equal or slightly shorter than T_1 in each case). Our measured results follow this trend. Notably, water's T_1 is orders of magnitude larger than those of glycerin and oil, as expected. Glycerin's T_2 is about 28 ms, shorter than its T_1, consistent with published glycerol T_2 values in the 20-40 ms range. Mineral oil's T_1 and T_2 are very similar (49 ms vs 44 ms), in line with the behavior of low-viscosity alkanes where $T_1 \approx T_2$.

The large differences in T_1 and T_2 between water, glycerin, and mineral oil can be explained by molecular mobility, viscosity, and hydrogen bonding. Water's small molecules reorient extremely fast (short correlation time), making its T_1 and T_2 very long because fast molecular motion weakens dipolar relaxation (the extreme motional narrowing limit). Glycerin's much higher viscosity ($\approx 1000\times$ that of water) means its molecules tumble slowly, which greatly enhances dipole-dipole relaxation efficiency — hence its T_1 is two orders of magnitude shorter. Additionally, glycerin's molecules form extensive hydrogen bonds that restrict motion and create strong local magnetic fields, causing very rapid dephasing ($T_2 \ll T_1$). Mineral oil is nonpolar and less viscous (intermediate mobility), so its relaxation times fall in between: T_1 and T_2 are on the order of 10^{-2}s. In fact, in low-viscosity liquids without strong intermolecular bonding, T_1 and T_2 are often similar. Glycerin, being viscous and H-bonded, shows T_2 much shorter than T_1 due to insufficient averaging of neighbor interactions. Water, with very low viscosity and transient H-bonds, has both T_1 and T_2 extremely high (on the order of seconds).

IV. CONCLUSION

In conclusion, the NMR relaxation times we measured reflect each liquid's molecular characteristics. Water showed a T_1 on the order of seconds ($\approx$1.9 s) and a long T_2 ($\approx$0.85 s), consistent with its highly mobile molecules and weak intermolecular constraints. Glycerin had much shorter T_1 ($\sim$40 ms) and T_2 ($\sim$28 ms), which is expected for a viscous, hydrogen-bonded liquid where slow molecular motion and strong dipolar interactions lead to fast relaxation. Mineral oil exhibited intermediate values (T_1 $\sim$49 ms, T_2 $\sim$44 ms), reflecting moderate molecular mobility and the absence of hydrogen bonding. These results agree well with published reference values (e.g. water T_1 $\sim$3 s, glycerin T_1 $\sim$45 ms). The trend (water $\gg$ oil $\geq$ glycerin in both T_1 and T_2) stems from fundamental physical differences: water's low viscosity and transient hydrogen bonds give it unusually prolonged spin relaxation, whereas glycerin's high viscosity and extensive hydrogen bonding dramatically accelerate spin-lattice and spin-spin relaxation. Thus, our findings illustrate how

increasing molecular size, stronger intermolecular forces, and higher viscosity lead to shorter T_1/T_2, while small, fast-diffusing molecules like water have exceptionally long relaxation times.

---

[1] D. J. Griffiths and D. F. Schroeter, *Introduction to Quantum Mechanics*, third edition ed. (Cambridge University Press, Cambridge ; New York, NY, 2018).

[2] Lab Manual, *Pulsed Nuclear Magnetic Resonance*.

[3] C. P. Slichter, *Principles of Magnetic Resonance*, 3rd ed. (Springer Science, USA, 1990).

Appendix A: Full-Size Purcell Plots for Mineral Oil, Glycerin, and DI Water

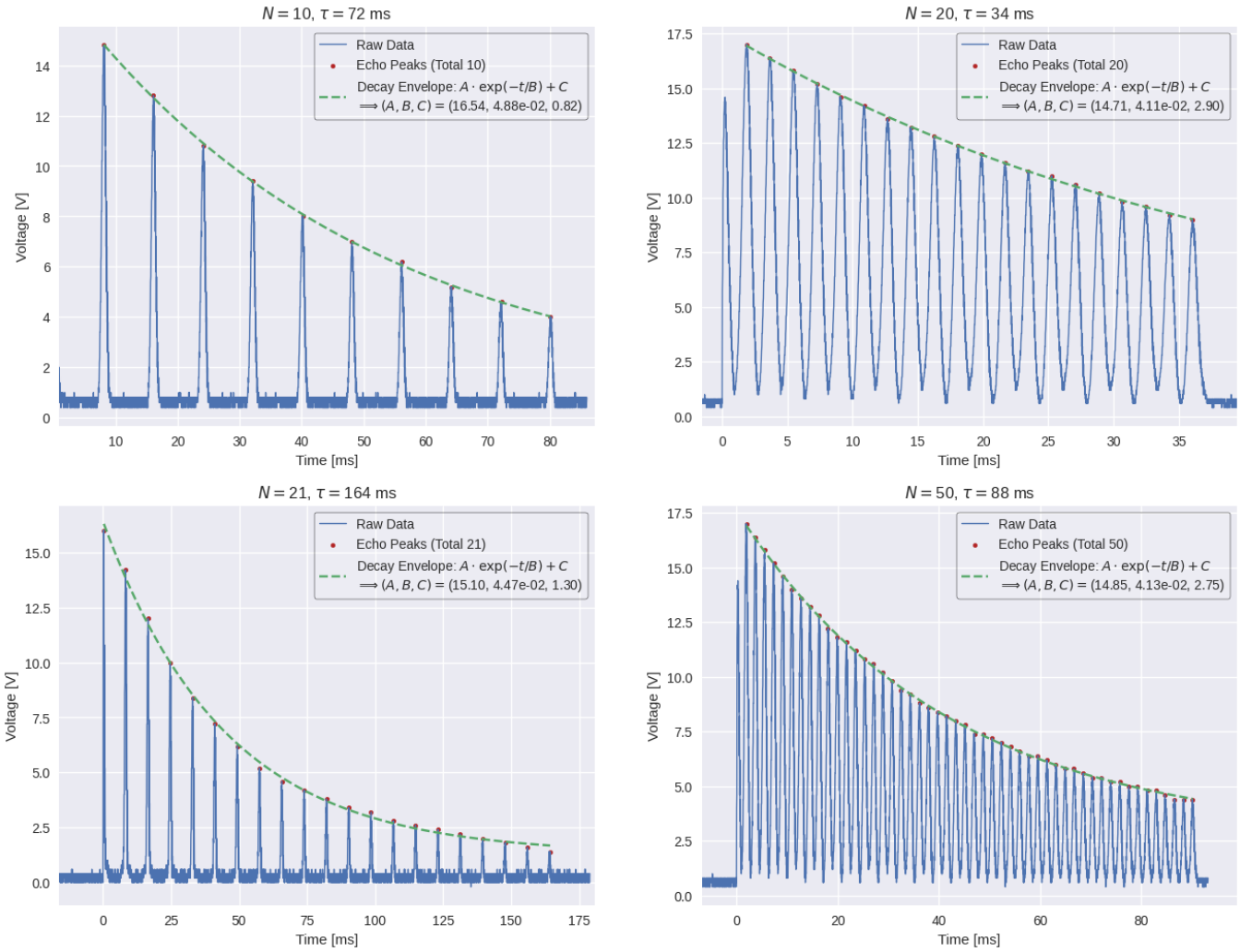

FIG. 5: Carr-Purcell sequences with various N, τ for mineral oil.

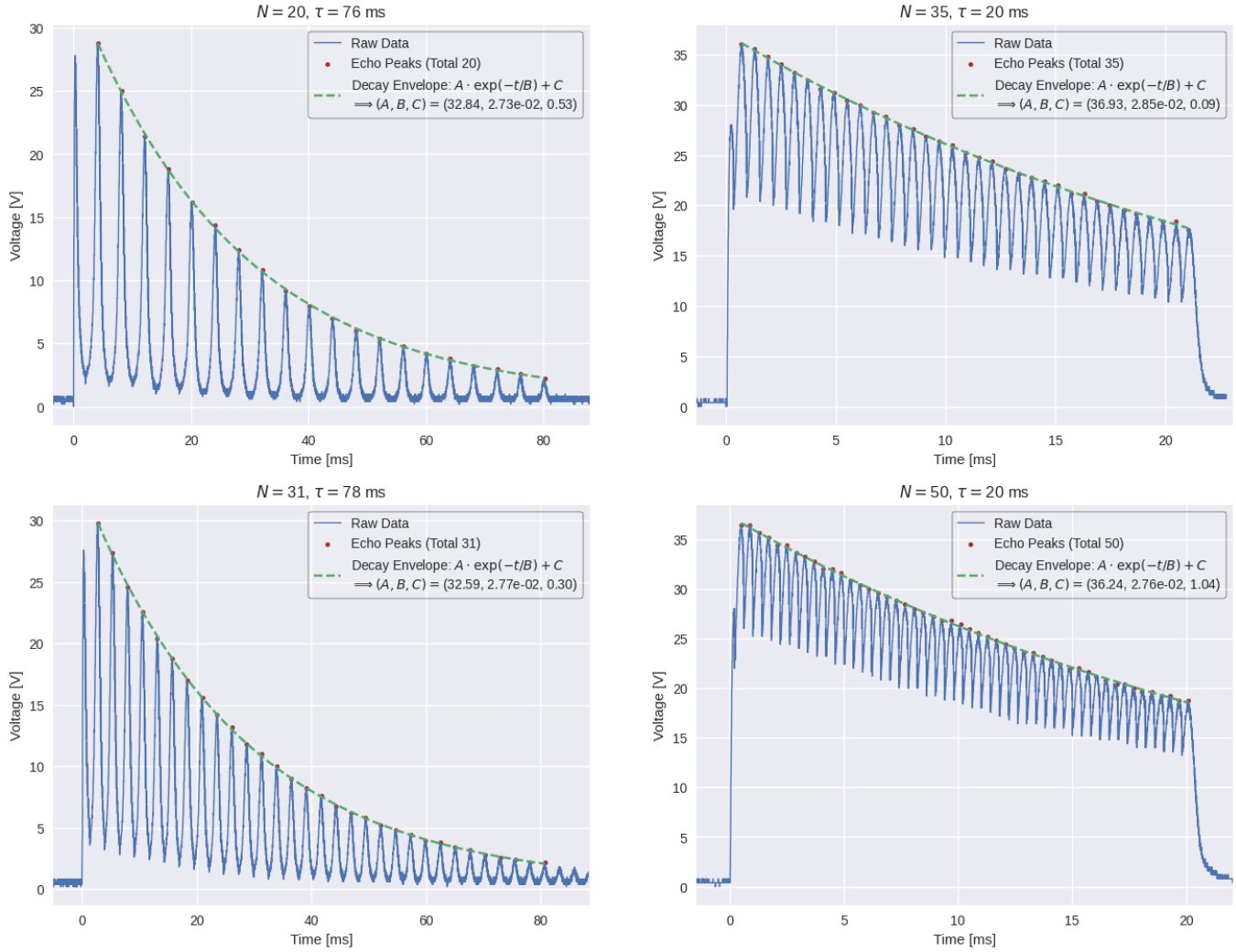

FIG. 6: Carr-Purcell sequences with various N, τ for glycerin.

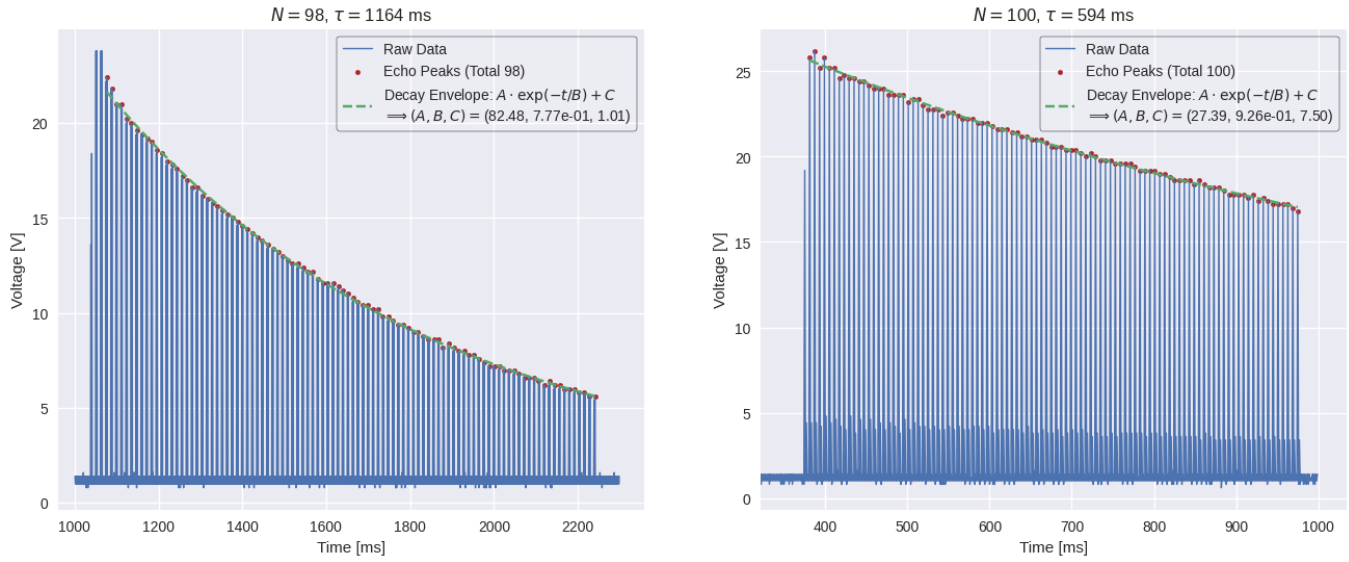

FIG. 7: Carr-Purcell sequences with various N, τ for deionized water.